Applied Physics A (2022) 128:893
https://doi.org/10.1007/s00339-022-06042-6

Applied Physics A
Materials Science & Processing

Development of fluoride-containing glass–ceramics using eggshells waste as calcium source

Zhi Wei Loh[1] · Wei Mun Cheong[1] · Mohd Hafiz Mohd Zaid[1,2] · Mohd Mustafa Awang Kechik[1] · Yap Wing Fen[1] · Mohd Zul Hilmi Mayzan[3] · Yazid Yaakob[1,4] · Shahira Liza[5]

Received: 21 June 2022 / Accepted: 7 September 2022 / Published online: 16 September 2022

Abstract

This paper reports on developing low-cost fluoride-containing glass–ceramics derived from eggshells waste as a source of calcium via the conventional melt-quenching method. The physical, structural, and mechanical properties of the samples before and after sintering is highlighted in this study. XRD and FTIR analysis confirmed the presence of fluorapatite, wollastonite, and cuspidine phases. It is worth noting that adding fluoride to the glass system would lead to the improvement of the mechanical properties of the final product. Among all, the sample sintered at 700 °C achieved the highest density and mechanical properties. It obtained a density value of 2.626 g/cm^3, a microhardness result of 6.72 GPa, and fracture toughness of 3.55 MPa·m$^{1/2}$. These results are better than commercial 45S5 bioglass (0.148 GPa–0.375 GPa) and comparable to the properties of human enamel (2.00 GPa–6.00 GPa). These findings would be believed to contribute to a low-cost waste-derived fluoride-containing glass–ceramics system in the dental application.

Keywords Glass–ceramics · Eggshells · Sintering · Melt-quenching · Mechanical properties

1 Introduction

Glass–ceramics, discovered by Stookey in the 1950s, are polycrystalline materials containing one or more crystal phases incorporated into a residual glass [1]. Glass–ceramics are fabricated from the glass of appropriate composition after undergoing controlled nucleation and crystallization through some sintering process [2]. Bioactive glass–ceramics are materials that have a biological reaction at the surface by forming a bond between the living tissue and the material. The common feature of the bioglass-ceramics is that their surface will develop biologically active hydroxyapatite (HA) layer that can bond to the hard and soft tissues such as bone. This HA phase mimics the mineral phase of bone and teeth [3, 4]. Recently, in response to the high demand for dental materials, the development of bioglass-ceramics materials with mechanical properties that match the human tooth and enamel is desirable [5]. Dental glass–ceramics materials are highly attractive due to their excellent physical and mechanical properties, for instance, wear resistance, high microhardness and fracture toughness [6]. However, glass–ceramics become more brittle with higher sintering temperature. Hence, selecting the right composition and optimal sintering temperature for the materials is still an interesting research topic to study and investigate.

It is worth mentioning that incorporating new ions into the bioglass system and undergoing controlled crystallization can improve the properties. Fluoride is an efficient material for reducing the chance of getting dental cavities by inhibiting enamel and dentine demineralization [7, 8]. Fluoride ions incorporated into the bioglass system will form

✉ Mohd Hafiz Mohd Zaid
mhmzaid@upm.edu.my

[1] Department of Physics, Faculty of Science, Universiti Putra Malaysia, UPM., 43400 Serdang, Selangor, Malaysia

[2] Material Synthesis and Characterization Laboratory, Institute of Advanced Technology, Universiti Putra Malaysia, UPM., 43400 Serdang, Selangor, Malaysia

[3] Ceramic and Amorphous Group (CerAm), Faculty of Applied Sciences and Technology, Pagoh Higher Education Hub, Universiti Tun Hussein Onn Malaysia, 84600 Panchor, Johor, Malaysia

[4] Department of Physical Science and Engineering, Graduate School of Engineering, Nagoya Institute of Technology, Gokiso-cho, Showa-ku, Nagoya 466-8555, Japan

[5] TriPrem I-Kohza, Malaysia-Japan International Institute Technology, Universiti Teknologi Malaysia, 54100 Kuala Lumpur, Malaysia

fluorapatite (FAp) instead of HA, where FAp is relatively more acid-resistant than HA. In addition, FAp is one of the main components of enamel and dentin and possesses antibacterial properties, making it more advantageous to apply in the dental application. Besides, fluoride can also enhance the materials' bone density and fracture toughness [9, 10]. Several studies have reported the influence of fluoride ions on bioglass and bioglass-ceramics. Lusvardi and their co-workers claimed that the formation of FAp after sintering highly depends on the phosphate content. The phosphate content of fluoride-containing bioglass-ceramics should not be less than 1.6 wt.% to have the appearance of FAp. [11, 12]. Zhao and the co-workers also reported that adding fluoride content to the glass system may lead to the densification and compactness of glass–ceramics. The F- ion will break the Si–O single-chain during crystallization, improving the crystallinity [13].

Hence, the present work aims to produce bioglass-ceramics where the properties are comparable to the desirable properties for dental application. Despite efforts to fabricate the bioglass-ceramics system, there are still limited studies on utilizing waste material as one of the compositions to fabricate the system. Therefore, this work also aims to synthesize the bioglass-ceramics system using eggshell waste as the calcium source as starting material. Besides, the studies on the physical, structural and mechanical properties of the fluoride-containing bioglass-ceramics after the sintering process will be evaluated.

2 Materials and methods

2.1 Glass–ceramics synthesis

The bioactive glass with the empirical formula $45SiO_2$-$25CaO$-$10B_2O_3$-$10Na_2O$-$4P_2O_5$-$6CaF_2$ was synthesized using the melt-quenching technique. The starting materials included eggshells waste as a calcium source, sodium carbonate (Na_2CO_3, Alfa Aesar, 99.5%) as Na_2O precursor, silicon dioxide (SiO_2, Commercial), boron oxide (B_2O_3, Acros Organics, 98%), phosphorus pentoxide (P_2O_5, Sigma-Aldrich) and calcium fluoride, (CaF_2, R&M Chemicals, 97%). First, the cleaned eggshells underwent a calcination process at 900 °C for 2 h to get the calcinated eggshell powder, CaO. The calcinated eggshell powder was ground, sieved into 45 µm powder form, and mixed with the other chemicals following the empirical formula. Then, the powder mixtures were transferred into an alumina crucible in the electric furnace for the melt and water quenching process at 1450 °C for 2 h (heating rate of 10 °C/min). Next, the obtained glass frits were crushed and sieved into a particle size of 45 µm powder form. The bioglass samples were then pressed into a 13 mm diameter size pellet. Lastly, the pellets were sintered at 600, 700, 800, and 900 °C for 2 h to study the bioglass and bioglass-ceramics samples' physical, structural and mechanical properties.

2.2 Glass–ceramics characterization

The density measurement is conducted using the Archimedes method for bioglass and bioglass-ceramics samples. At least five measurements were taken to get the average density provided with the estimated error of ± 0.001 g/cm^3. The equation for density can be defined as below:

$$\rho_{glass} = \left(\frac{w_{air}}{w_{air} - w_{water}}\right)\rho_{water} \quad (1)$$

where w_{air} = the weight of sample in the air, w_{water} = the weight of sample in water, and ρ_{water} = the density of water which is 1.00 g/cm^3.

The amorphous nature structure of the bioglass and the crystalline phase existence in the bioglass-ceramics were identified using X-ray diffraction (XRD, X'Pert PRO MPD diffractometer, PANalytical, Philips; Cu-Kα radiation = 1.5406 Å; 40 kV and 40 mA; range from 20° to 80°). The results of the samples were determined by comparing them with the Inorganic Crystal Structure Database (ICSD). The chemical bonding of the bioglass and bioglass-ceramics were determined using Fourier Transform Infrared (FTIR) spectrometer (Spectrum 100 series, Perkin Elmer) in wavenumber 400 to 4000 cm^{-1}. The cross-section surface morphology and microstructure of the bioglass and bioglass-ceramics were analyzed using COXEM EM-30AX scanning electron microscopy (SEM). The samples were mounted on the stainless steel stab using standard carbon tap and gold coated avoid the electorstatic charge during the scanning process.

The compressive strength test (CST) and Vickers microhardness (HV) measurements were obtained to study the mechanical properties of the bioglass and bioglass-ceramics samples. Compressive strength was performed using Instron 3366 Dual Column Universal Test System (10kN load cell; crosshead of 1 mm/min). Vickers microhardness measurements were performed on the samples' surface by pressing a load of 4.905 N (HV 0.5) for 15 s. At least five readings will be taken to get the average results on each bioglass and bioglass-ceramics sample. The microhardness was calculated using the formula below:

$$HV = 1.854\left(\frac{2P\sin\frac{\theta}{2}}{D^2}\right) \quad (2)$$

where P = applied load in kgf, D = mean diagonal of the indentation in mm, and θ = angle between the opposite faces of the diamond (136°). After obtaining the microhardness

values, the fracture toughness was calculated using the Nihara formula [14] denoted as below:

$$K_{IC} = 0.203\left(\frac{c}{a}\right)^{-\frac{3}{2}} \cdot HV \cdot a^{\frac{1}{2}} \quad (3)$$

where K_{IC} = the fracture toughness value, a = the half-length of the indentation, c = the half-length of the crack, and HV = the Vickers microhardness value.

3 Result and discussion

3.1 XRF analysis

The chemical composition of the eggshells powder after calcination is presented in Table 1. The CaO produced from the eggshells after calcinated at 900 °C for 2 h is 97.90%. Previous researchers have reported that this is the suitable temperature and duration to obtain the highest purity of the CaO composition [15, 16]. Hence, CaO extracted from eggshells is considered as an alternative source to replace the commercial CaO as the eggshells are eco-friendly and cheaper, which could help to reduce the production cost.

3.2 Density analysis

Figure 1 shows the density measurement of bioglass and bioglass-ceramics with various sintering temperatures. The bioglass without sintering is denoted as 30 °C. As can be seen in Fig. 1, the density increases from 2.168 g/cm^3 to 2.626 g/cm^3 with the increment of sintering temperature up to 700 °C. The result is related to the densification process that took place, making the samples' structure more compact and dense with the increase in sintering temperature [17]. Further increasing the sintering temperature to 900 °C, there is a fall in the density from 2.440 g/cm^3 to 2.012 g/cm^3. The decreasing trend might be due to the rapid diffusion of the particle stimulating the crystal to grow, which inhibits the densification of the glass–ceramics [18]. Hence, the sample with 700 °C showed the highest density among all the samples.

Table 1 Chemical compositions of the eggshells powder after calcination

Chemical composition	Weight percentage, %
CaO	97.9000
MgO	0.9030
Na_2O	0.1540
Al_2O_3	0.1430
SiO_2	0.1400
P_2O_5	0.4040
SO_3	0.2200
K_2O	0.0436
Others	0.0924
Total	100.0000

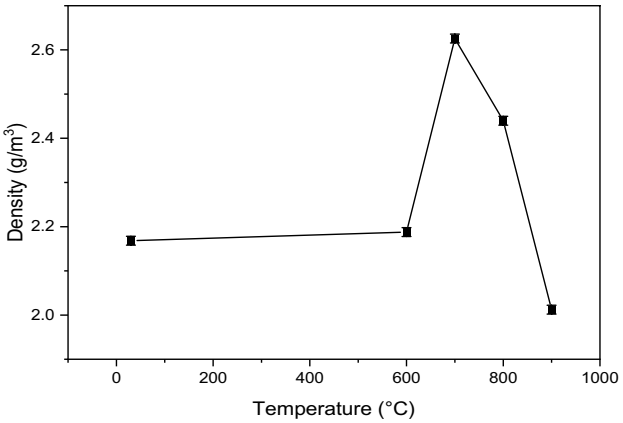

Fig. 1 Density measurement of bioglass and bioglass-ceramics with various temperatures

3.3 XRD analysis

XRD analysis is conducted on the bioglass and bioglass-ceramics to confirm the amorphous nature and identify the presence of crystalline phases after the sintering process. Figure 2 shows the XRD patterns of the bioglass and bioglass-ceramics with various temperatures. From the Fig. 2, it can be seen that there are no sharp peaks detected for the bioglass and bioglass sintered at 600 °C, showing the amorphous nature of the glass structure of the samples. It can be noticed that the phase compositions of the bioglass sintered at 700 °C belong to fluorapatite (ICSD 89–006-5266) and cuspidine (ICSD 98-002-1508) with a minor phase of silicon dioxide (ICSD 98–003-3030). Fluorapatite (FAp) containing glass–ceramics is a bioactive compound with an apatite-like structure, where the OH groups are replaced by fluorine. FAp is claimed that it can increase the hardness as well as protect the samples against the effect of lower pH in the oral cavity [19].

Furthermore, it is observed that the appearance of the wollastonite (ICSD 98–004-6164) phase and the characteristic peaks of fluorapatite increase significantly with the increment of sintering temperatures up to 900 °C. This variation of phase compositions is mainly due to the sintering temperature that would enhance the atomic mobility, leading to the grain growth and resulting in better crystallinity of the samples [20]. Similar results from Sujirote and the co-workers where the formation of the cuspidine phase will transform into wollastonite at higher sintering temperature with the addition of fluoride [21]. The presence of the wollastonite phase in the samples provides good strength and

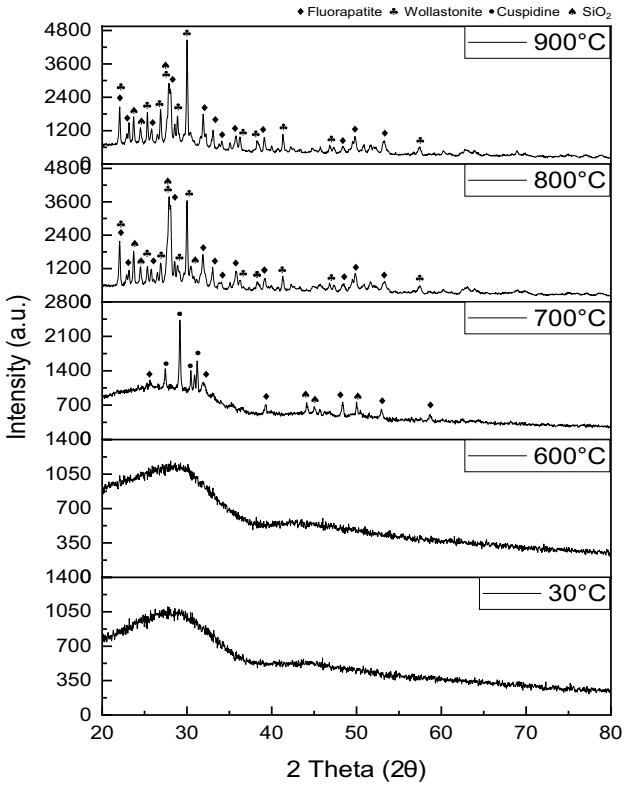

Fig. 2 XRD patterns of bioglass and bioglass-ceramics with various sintering temperatures

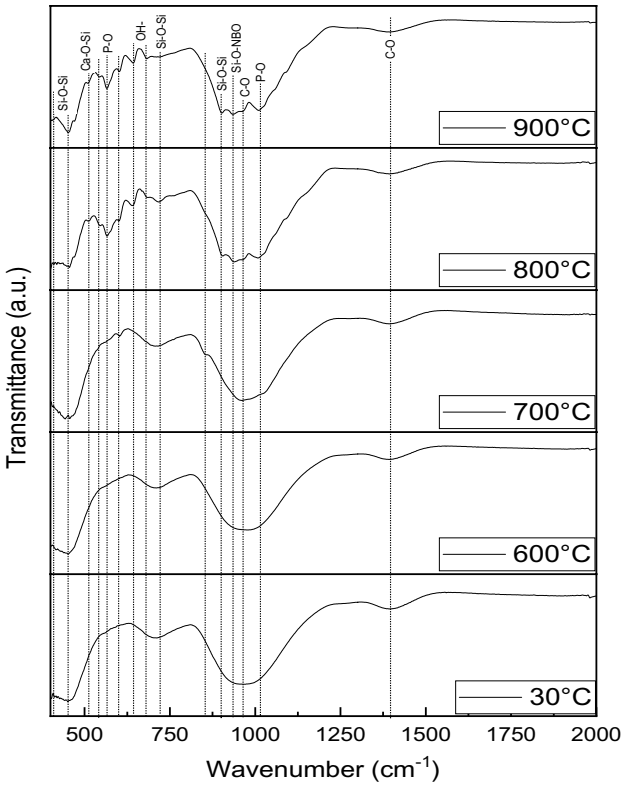

Fig. 3 FTIR spectra of bioglass and bioglass-ceramics with various sintering temperatures

will not affect the bioactivity of the final product. Hence, the crystal phase formation of the samples is highly dependent on the composition stoichiometry and sintering behavior.

3.4 FTIR analysis

FTIR analysis is a common technique for identifying the glass structure, and it is claimed to be an effective tool for detecting the glass crystallization after sintering [22]. Figure 3 presents the FTIR spectra of bioglass before and after sintering with various temperatures. The assignments of vibrations modes and the band's position for the samples' FTIR spectra are gathered and compiled in Table 2. The absorption band for the samples without sintered and after sintered at 600 °C are situated in the range of 400–470 cm^{-1}, 530–600 cm^{-1}, 650–800 cm^{-1}, and 850–1150 cm^{-1}. The broad width of the absorption band reflects the characteristic of the glass structure. Further raising the sintering temperature to 700 °C, the formation of a new absorption band appeared at 852 cm^{-1}, which belonged to the Cuspidine structure [23]. This finding can be proven by the result of the XRD analysis. Furthermore, when the sample sintered up to 900 °C, it is worth to note that there are more absorption bands and shifting bands in the figure, showing the presence of crystalline phases in the sample network. From the figure, the absorption band located at 422–453 cm^{-1} and 400–600 cm^{-1} are attributed to the Si–O–Si bending vibrational mode [24] and Ca–O stretching vibrational mode [25]. The band at 512 cm^{-1} is attributed to the Si–O–Si bending vibrational mode [26] that forms the Ca–O–Si bond [27].

Table 2 FTIR spectral band assigned to the vibrational modes

Wavenumbers (cm^{-1})	Assignment of vibrational mode	References
~422–453	Si–O–Si bending mode	[24]
~400–600	Ca–O stretching mode	[25]
~512	Si–O–Si bending mode Ca–O–Si mode	[26] [27, 42]
~539–565, ~598	P–O bending mode	[34, 35]
~641–681	OH- vibrational mode	[31]
~720	P–O–P symmetric stretching mode Si–O–Si stretching mode	[37] [28]
~902	Si–O–Si stretching mode	[29]
~934	Si–O–NBO stretching mode	[30]
~965	C–O bending mode	[39]
~1015	P–O stretching mode Si–O-Si asymmetric stretching mode	[36] [38]
~1397	C–O stretching mode	[40]

The appearance of the intense absorption bands at higher sintering temperatures indicated the formation of wollastonite crystal phases in the sample structure. Besides, some new bands at 720 cm^{-1} and 902 cm^{-1} that emerged in the absorption spectra are assigned to the Si–O–Si symmetric stretching vibration mode [28, 29], where the band at 934 cm^{-1} is assigned to the Si–O–NBO symmetric stretching vibration mode [30].

Moreover, the presence of OH vibrational mode located in 641–681 cm^{-1} suggested that the hydroxyl groups in fluorapatite samples were substituted by the fluoride ions [31]. The similar observations presented by Freund and Knobe, and Rintoul and the teams mentioned that the absorption spectra falls in the 630–750 cm^{-1} region indicated the appearance of –OH groups in the –OH···F bonds in the fluorapatite spectra [32, 33]. Apart from that, the P–O bending vibrational mode [34, 35] and P–O stretching vibrational mode [36] are located at 539–565 cm^{-1}, 598 cm^{-1}, and 1015 cm^{-1}, are referred to the presence of crystalline phosphate in the apatite formation. Another band situated in 720 cm^{-1} is related to the superposition of P–O–P and Si–O–Si symmetric stretching vibration mode in the apatite spectra, as suggested by Abo-Naf and the co-workers [37]. On the other hand, the band located at 1015 cm^{-1} with the increasing sintering temperature can be referred to as the overlapping of P–O symmetric and Si–O–Si asymmetric stretching vibration mode [38]. It can be observed that the weak bands located at 965 cm^{-1} and 1397 cm^{-1} are related to the C–O bending [39] and stretching [40] vibrational group, respectively. The results can be explained by the presence of the carbonate ion in the apatite phase. There might also be due to the decomposition of calcium carbonate and sodium carbonate used in the glass samples [41]. Since the FTIR spectra for both phases are different, the absorption spectra can detect the formation of FAp spectra instead of HA spectra in this study.

3.5 SEM analysis

Figure 4 illustrates the SEM micrographs of the bioglass and bioglass-ceramics with various sintering temperatures using the magnification of 1000x. Generally, the evolution of the microstructure happened with the progression of sintering temperatures. From Fig. 4a and b, it can be seen that the micrographs show the non-uniform particle distribution with irregular shapes, indicating the amorphous glass structure. Increase the sintering temperature to 700 °C, the sample consolidated and possessed densification, showing fewer pores and vacant areas in the sample, as shown in Fig. 4c. This confirmed the effectiveness of the sintering process [43]. Meanwhile, Fig. 4d and e show the micrographs of the samples with the presence of pores. The large pores are likely related to the porosity created by the decomposition of $CaCO_3$ with the CO_2 gasses trapped in the samples, which

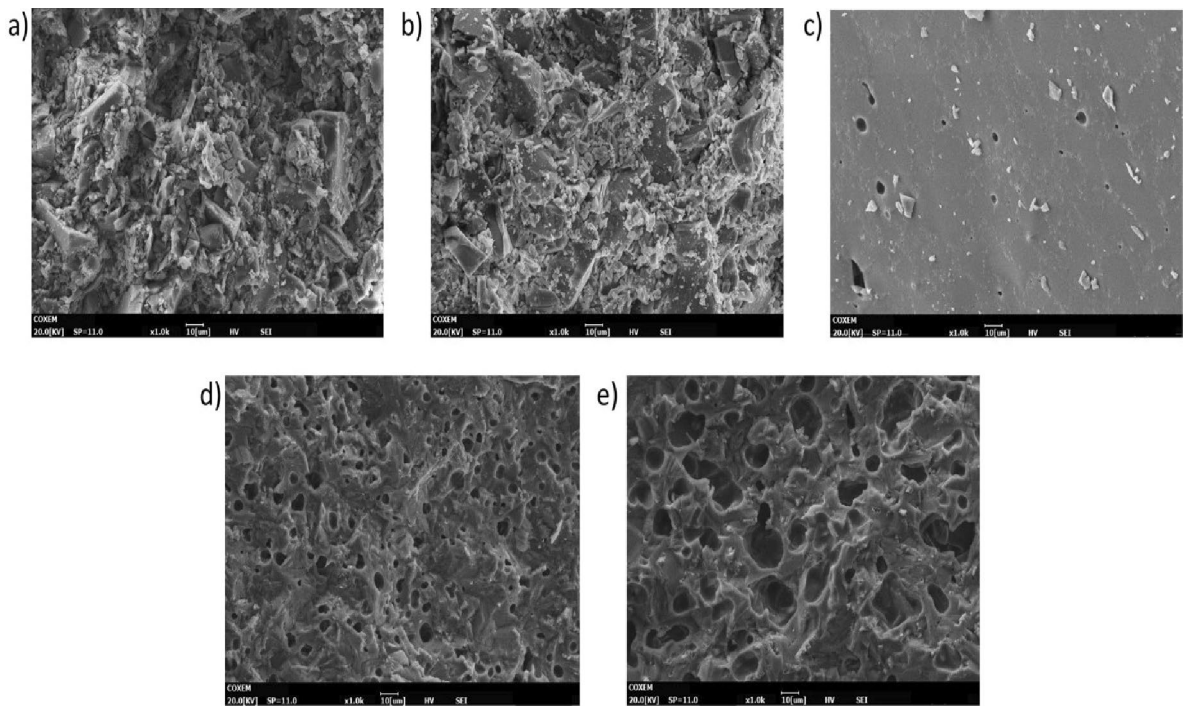

Fig. 4 SEM micrographs of bioglass and bioglass-ceramics with various sintering temperatures at 1000× magnification for (**a**) 30 °C, (**b**) 600 °C, (**c**) 700 °C, (**d**) 800 °C and (e) 900 °C

takes place at a temperature where the viscosity facilitates the expansion of the samples [42, 44]. The porosity that presence in the samples would affect the mechanical properties of the final products.

3.6 Compressive strength analysis

Strength is a crucial criterion for studying the mechanical properties of the samples as final dental materials. Basically, the average load during the normal chewing process is reported in the wide range from 6 to 440 N [45]. Higher strength to withstand the tension from the load is more favorable for dental application. Figure 5 shows the compressive strength results of the bioglass and bioglass-ceramics with various sintering temperatures. From the Fig. 5, the compressive strength of the sample increases from 48.98 ± 0.05 MPa to 73.84 ± 0.14 MPa as the increment of sintering temperature up to 700 °C. The increase in compressive strength performance is mainly caused by the occurrence of crystallization and densification of the bioglass, leading to the compactness of the samples, which has a similar result as the density measurement. Zhao and the research team reported that the appearance of fluorapatite and the cuspidine phase would enhance the mechanical properties of the final sample [13]. However, raising the sintering temperature to 900 °C showed an adverse result, as the bioglass-ceramics sample might become more brittle with a higher sintering temperature. The decrease in mechanical properties from the results when the sintering temperature increases from 800 °C to 900 °C might be related to the formation of more phases during crystallization, increasing the size of the pores in the samples. Hence, this results in weak compressive strength compared to the other samples. Therefore, choosing the optimum temperature to get better properties of the final product is still very challenging.

3.7 Vickers microhardness and fracture toughness analysis

Another crucial mechanical features for testing on long-term dental materials include microhardness and fracture toughness analysis. The quality of the final product is highly dependent on the high hardness value of the material, which is similar to human enamel [46]. Figure 6 presents the Vickers microhardness of the bioglass and bioglass-ceramics with various sintering temperatures. The figure shows an increasing graph when the sintering temperature goes up to 700 °C and a decreasing graph from 800 °C to 900 °C. Among all the temperatures, the sample sintered at 700 °C reveals the highest microhardness value, 6.72 ± 0.03 GPa. The high microhardness result might relate to the increase in sintering temperature, leading to the compactness of the samples. Besides, adding fluorine helps improve the mechanical properties of the samples [47]. The microhardness of the produced samples (3.09 GPa – 6.72 GPa) is significantly higher than the microhardness of 45S5 commercial bioglass (0.148 GPa – 0.375 GPa) [48] and comparable to that of the human enamel (2.00 GPa – 6.00 GPa) [49].

On the other hand, Fig. 7 presents the fracture toughness of the bioglass and bioglass-ceramics with various sintering temperatures. Among all the results, the sample sintered at 700 °C obtained the optimal fracture toughness value of 3.55 ± 0.15 MPa·m$^{1/2}$. Although the fracture toughness of the samples is not that high, it is still higher than that of 45S5 commercial bioglass (0.50 MPa·m$^{1/2}$ – 1.00 MPa·m$^{1/2}$) [50] and closer to that of the human enamel (0.67 MPa·m$^{1/2}$ – 3.97 MPa·m$^{1/2}$) [51]. The fracture toughness of dental

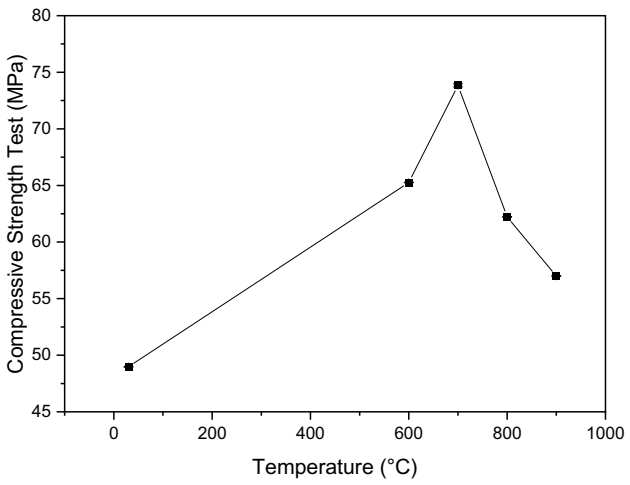

Fig. 5 The compressive strength of bioglass and bioglass-ceramics with various sintering temperatures

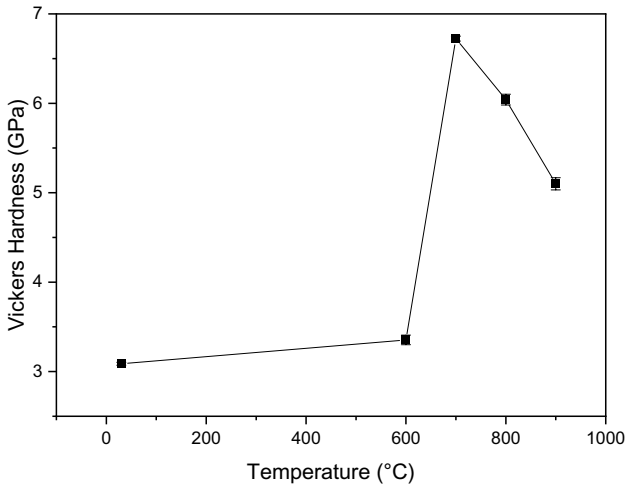

Fig. 6 Vickers microhardness of bioglass and bioglass-ceramics with various sintering temperatures

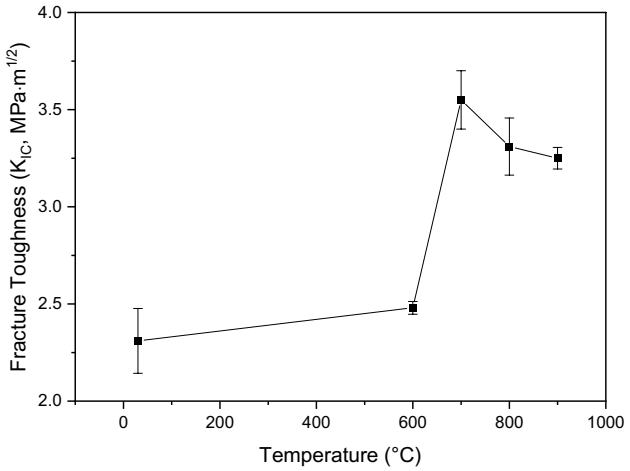

Fig. 7 Fracture toughness of bioglass and bioglass-ceramics with various sintering temperatures

material is a significant concern in dentistry application. The resistance to fracture is the main requirement for most structural materials [52]. Hence, choosing the suitable composition and sintering temperature have to be considered to get better characteristics of the final product to be applied in the dental application.

4 Conclusion

This study shed light on developing low-cost fluoride-containing glass–ceramics derived from eggshells waste as a calcium source via conventional melt-quenching technique. As a result, the dense and sinter-crystallized materials were successfully produced through the sintering process. The XRF analysis confirmed the purity of CaO in the calcinated eggshells. The XRD and FTIR results confirmed the presence of fluorapatite, wollastonite, and cuspidine phases. Among the investigated materials, the sample with a sintering temperature of 700 °C obtained the highest density value, compressive strength, microhardness, and fracture toughness. The obtained results are similar and comparable to the properties of the human enamel. These features qualify the produced samples for further investigation as potential candidates for dental application.

Acknowledgements This research was supported by the Universiti Putra Malaysia through the Geran Putra Berimpak (GP-GPB/2021/9702600) for this research work.

Author contribution ZWL: conceptualization, methodology, software, formal analysis, investigation, data curation, writing—original draft, visualization. WMC: conceptualization, methodology, software, formal analysis, investigation. MHMZ: conceptualization, methodology, formal analysis, data curation, writing—original draft, supervision, project administration, funding acquisition. MMAK, YWF: formal analysis, data curation, writing—review & editing, supervision. data curation, writing—review & editing. MZHM, YY, SL: methodology, software, formal analysis, data curation.

Declarations

Competing interest The authors declared that they have no conflicts of interest to this work.

References

1. J. Deubener, M. Allix, M.J. Davis, A. Duran, T. Höche, T. Honma, T. Komatsu, S. Krüger, I. Mitra, R. Müller, S. Nakane, M.J. Pascual, J.W.P. Schmelzer, E.D. Zanotto, S. Zhou, J. Non. Cryst. Solids **501**, 3 (2018)
2. S.S. Owoeye, S.M. Abegunde, D.O. Folorunso, B.O. Adigun, U. Kingsley **5**, 100062 (2021)
3. M. Montazerian, E.D. Zanotto, *in Bioactive glasses: Fundamentals, technology and applications* (Royal Society of Chemistry, Cambridge, 2017)
4. S. Balhuc, R. Campian, A. Labunet, M. Negucioiu, S. Buduru, A. Kui, Curr. Comput.-Aided Drug Des. **11**, 1 (2021)
5. E. Fiume, G. Magnaterra, A. Rahdar, E. Verné, F. Baino, Ceramics **4**, 542 (2021)
6. K. Dimitriadis, A.K. Sfikas, S. Kamnis, P. Tsolka, S. Agathopoulos, J. Adv. Prosthodont. **14**, 96 (2022)
7. M.S. Dahiya, V.K. Tomer, S. Duhan, *Applications of Nanocomposite Materials in Dentistry* (Elsevier, Amsterdam, 2018)
8. R. Ramadoss, R. Padmanaban, B. Subramanian, J. Biomed. Mater. Res. - Part B Appl. Biomater. **110**, 45 (2022)
9. D.S. Brauer, M.N. Anjum, M. Mneimne, R.M. Wilson, H. Doweidar, R.G. Hill, J. Non. Cryst. Solids **358**, 1438 (2012)
10. N.A. Al-eesa, S.D. Fernandes, R.G. Hill, F.S.L. Wong, U. Jargalsaikhan, S. Shahid, Dent. Mater. **37**, 672 (2021)
11. G. Lusvardi, G. Malavasi, L. Menabue, V. Aina, C. Morterra, Acta Biomater. **5**, 3548 (2009)
12. S. N. F. S. Adam, F. Zainuddin, and A. F. Osman, J. Phys. Conf. Ser. **2080**, (2021).
13. S.Z. Zhao, X.Y. Zhang, B. Liu, J.J. Zhang, H.L. Shen, S.G. Zhang, Rare Met. **40**, 3316 (2021)
14. K. Harada, A. Shinya, H. Gomi, Y. Hatano, A. Shinya, A.J. Raigrodski, J. Prosthet. Dent. **115**, 215 (2016)
15. R. Rohim, R. Ahmad, N. Ibrahim, N. Hamidin, C.Z.A. Abidin, Adv. Environ. Biol. **8**, 35 (2014)
16. R. Mohadi, K. Anggraini, F. Riyanti, A. Lesbani, Sriwij. J. Environ. **1**, 32 (2016)
17. A.A.W. Rabiatul, M.H.M. Zaid, K.A. Matori, M.K. Halimah, N.A.M. Yamin, S.N.F. Zalamin, N.A.N. Ismail, S. Honda, M. Tanemura, Macromol. Symp. **401**, 2100316 (2022)
18. W. Di Fan, B. Liu, X. Luo, J. Yang, B. Guo, S.G. Zhang, Rare Met. **38**, 245 (2019)
19. K. Pajor, L. Pajchel, J. Kolmas, Materials (Basel). **12**, 1 (2019)
20. H. Chen, Q. Sun, J. Zhang, and J. Sheng, Ceram. Int. **48**, 20400–20408 (2022)
21. K. Sujirote, R.D. Rawlings, P.S. Rogers, J. Eur. Ceram. Soc. **18**, 1325 (1998)
22. J. Partyka, M. Leśniak, Spectrochim. Acta - Part A Mol. Biomol. Spectrosc. **152**, 82 (2016)
23. Z. Luo, F. He, W. Zhang, Y. Xiao, J. Xie, R. Sun, M. Xie, Mater. Chem. Phys. **242**, 122531 (2020)

24. C. Wen, N. Bai, L. Luo, J. Ye, X. Zhan, Y. Zhang, and B. Sa, Ceram. Int. 1 (2021).
25. D.I. Saparuddin, N.A. Noor Hisham, S.A. Aziz, K.A. Matori, S. Honda, Y. Iwamoto, M.H. Mohd Zaid, J. Mater. Res. Technol. **9**, 5640 (2020)
26. S. Palakurthy, K.V. Reddy, S. Patel, P.A. Azeem, Prog. Biomater. **9**, 239 (2020)
27. M.A. Mahdy, I.K. El Zawawi, S.H. Kenawy, E.M.A. Hamzawy, G.T. El-Bassyouni, Ceram. Int. **48**, 7218 (2022)
28. A. Charmforoushan, M.R. Roknabadi, N. Shahtahmassebi, B. Malaekeh-Nikouei, M. Bagherabadi, Mater. Chem. Phys. **280**, 125825 (2022)
29. P. Paramita, M. Ramachandran, S. Narashiman, S. Nagarajan, D.K. Sukumar, T.W. Chung, M. Ambigapathi, J. Mater. Sci. Mater. Med. (2021). https://doi.org/10.1007/s10856-020-06478-3
30. L. de Siqueira, T.M.B. Campos, S.E.A. Camargo, G.P. Thim, E.S. Trichês, J. Non. Cryst. Solids **555**, 120629 (2021)
31. L. Borkowski, A. Przekora, A. Belcarz, K. Palka, G. Jozefaciuk, T. Lübek, M. Jojczuk, A. Nogalski, G. Ginalska, Mater. Sci. Eng. C **116**, 111211 (2020)
32. F. Freund, M. Knobel, W. Germany, S. Ingram, D. M. Adams, I. R. Gardner, G. Schaeken, M. H. Verbeek, F. C. M. Driessens, B. L. Ingram, and I. May, **11**, 1136–1140 (1973)
33. L. Rintoul, E. Wentrup-Byrne, S. Suzuki, L. Grøndahl, J. Mater. Sci. Mater. Med. **18**, 1701 (2007)
34. S. Amudha, J.R. Ramya, K.T. Arul, A. Deepika, P. Sathiamurthi, B. Mohana, K. Asokan, C.L. Dong, S.N. Kalkura, Compos. Part B Eng. **196**, 108099 (2020)
35. F. Sharifianjazi, M. Moradi, A. Abouchenari, A.H. Pakseresht, A. Esmaeilkhanian, M. Shokouhimehr, M. Shahedi Asl, Ceram. Int. **46**, 22674 (2020)
36. X. Lu, J. Kolzow, R.R. Chen, J. Du, Bioact. Mater. **4**, 207 (2019)
37. S.M. Naf, E.S.M. Khalil, E. Sayed, H.A. Zayed, R.A. Youness, Spectrochim. Acta - Part A Mol. Biomol. Spectrosc **144**, 88 (2015)
38. E.M.A. Khalil, R.A. Youness, M.S. Amer, M.A. Taha, Ceram. Int. **44**, 7867 (2018)
39. N. Montazeri, R. Jahandideh, E. Biazar, Int. J. Nanomedicine **6**, 197 (2011)
40. V. Uskoković, G. Abuna, P. Ferreira, V.M. Wu, L. Gower, F.C.P. Pires-de-Souza, R.M. Murata, M.A.C. Sinhoreti, S. Geraldeli, J. Sol-Gel Sci. Technol. **97**, 245 (2021)
41. N.A.N. Hisham, M.H.M. Zaid, K.A. Matori, M.K. Shabdin, Mater. Sci. Eng. B **281**, 115730 (2022)
42. N.F.B. Pallan, K.A. Matori, M. Hashim, R.S. Azis, N. Zainuddin, N.F.B. Pallan, F.M. Idris, I.R. Ibrahim, L.C. Wah, S.N.A. Rusly, N. Adnin, M.Z.A. Khiri, Z.N. Alassan, N. Mohamed, M.H.M. Zaid, Sci. Sinter. **51**, 377 (2019)
43. D. Bellucci, E. Veronesi, M. Dominici, and V. Cannillo, Mater. Sci. Eng. C **110**, 110699 (2020)
44. F.A. da Silva Fernandes, S. Arcaro, E.F. Tochtrop Junior, J.C. Valdés Serra, C.P. Bergmann, Process. Environ. Prot. **128**, 77 (2019)
45. L. Fu, H. Engqvist, W. Xia, Materials (Basel). **13**, 1 (2020)
46. N.D. Yanikoglu, R.E. Sakarya, J. Mater. Res. Technol. **9**, 9720 (2020)
47. D.S. Brauer, N. Karpukhina, R.V. Law, R.G. Hill, J. Mater. Chem. **19**, 5629 (2009)
48. N.M. Possolli, D.F. da Silva, J. Vieira, N. Maurmann, P. Pranke, K.B. Demétrio, E. Angioletto, O.R.K. Montedo, S. Arcaro, J. Biomed. Mater. Res. - Part B Appl. Biomater. **110**, 67 (2022)
49. J.W. Nicholson, S.K. Sidhu, B. Czarnecka, Materials (Basel). **13**, 1 (2020)
50. M. Nizam Uddin, R. Asmatulu, *Synthesis, Characterization, and Applications of Polymer Based Biomaterials* (Nova Science Publishers Inc, New York, 2019)
51. K. Dimitriadis, K.C. Vasilopoulos, T.C. Vaimakis, M.A. Karakassides, D.U. Tulyaganov, S. Agathopoulos, Int. J. Appl. Ceram. Technol. **17**, 2025 (2020)
52. M. Yahyazadehfar, J. Ivancik, H. Majd, B. An, D. Zhang, D. Arola, Appl. Mech. Rev. **66**, 1 (2014)